The predictability of shallow landslides: lessons from a natural laboratory

R. Bainbridge[1], M. Lim[2], S. Dunning[1], M.G. Winter[3], A. Diaz-Moreno[1], J. Martin[2], H. Torun[2], B. Sparkes[4], M. Khan[2], N. Jin[2]

[1] Department of Geography, Newcastle University, Newcastle, NE1 7RU, UK

[2] Department of Geography, Northumbria University, Newcastle, NE1 8SB, UK

[3] Winter Associates, Kirknewton, Midlothian, EH27 8AF, UK

[4] Richard Allitt Associates Ltd, The Forge Offices, Haywards Heath, RH17 6ET, UK

Corresponding author: rupert.bainbridge@ncl.ac.uk

The predictability of shallow landslides: lessons from a natural laboratory

R. Bainbridge[1], M. Lim[2], S. Dunning[1], M.G. Winter[3], A. Diaz-Moreno[1], J. Martin[2], H. Torun[2], B. Sparkes[4], M. Khan[2], N. Jin[2]

[1] *Department of Geography, Newcastle University, Newcastle, NE1 7RU, UK*

[2] *Department of Geography, Northumbria University, Newcastle, NE1 8SB, UK*

[3] *Winter Associates, Kirknewton, Midlothian, EH27 8AF, UK*

[4] *Richard Allitt Associates Ltd, The Forge Offices, Haywards Heath, RH17 6ET, UK*

ABSTRACT

Shallow landslides are a significant hillslope erosion mechanism and can transform into destructive debris-flows. Limited understanding of the controls on debris-flow initiation, development and deposition results in persistent risk and high impacts where linear infrastructure is affected. Here, we analyse steep slopes above a key road, the A83 Rest and be Thankful, Scotland, where near-real-time rain gauge data, time-lapse camera deformation tracking and seismics allow us to define thresholds for increased debris-flow risk, examine long-term slope creep and, detect debris-flow occurrence. We show the patterns and development of channelized and hillslope debris-flows that act as a key geomorphic agent, accounting for 58% of landslide source volume over 13-years. On-slope rainfall data allow us to quantify the effect of antecedent rainfall and storm intensity-duration on landslide triggering and develop new local thresholds over which landslides are likely to occur. To better equip asset managers, we use time-lapse imagery vector tracking to detect slope instabilities, and deformation rates to calculate inverse-velocity values to indicate if

failure is imminent. Low-cost seismometers are used to detect when a debris-flow has occurred and locate the source area. The suite of sensors has provided vital information both prior to failure, and during debris-flows to support operational decision-making for authorities dealing with complex slope hazards.

INTRODUCTION

Debris-flows are extremely rapid (>5 m/s), saturated debris landslides from hillslopes (Hungr et al., 2014). Shallow landslides translate into debris-flows given favourable material and fluidisation conditions (Zimmerman et al., 2020). Debris-flow runout potential and capacity to entrain water and sediment make them a significant global hazard, particularly where linear infrastructure traverses affected slopes (Geertsema et al., 2009; Meyer et al., 2015). They can be broadly grouped into channelized debris-flows (CDFs) that are constrained for their flow path and hillslope debris-flows (HDFs) that occur on non-incised slopes (Chen et al., 2009). CDFs and HDFs can transition into one another where HDFs meet gullies or CDFs breach channels and flow over slope; hillslope-gully coupling controls the hazard potential (Milne et al., 2009). CDFs often occur in torrent systems, such as the Illgraben, Switzerland (Badoux et al., 2009) where the repeated flow path removes some of the risk uncertainty.

Where debris-flows source across large areas with uncertain runout, a combination of active mitigation (physically controlling site aspects using engineering infrastructure) and passive mitigation (reducing impacts via land-use planning, closures and warning systems) methods can be used (Huebl and Fiebiger, 2005; Vagnon, 2020).

In Scotland, debris-flows have repeatedly damaged linear infrastructure resulting in economic and social costs (Winter et al. 2019a). Here we demonstrate the use of near-real-time, on-site data to supplement Landslide Management Plans (LMP) and enhance alert capabilities for stakeholders at a debris-flow prone slope in the west of Scotland.

STUDY AREA

The A83 Rest and be Thankful (RabT), a key road into west Scotland, has the highest landslide frequency on the Scottish road network (McMillan and Holt, 2019). It bisects the south-western slope of Beinn Luibhean above Glen Croe. The bedrock is Schist, with overlying till up to 3 m thick, interspersed with gullies, scars, levees and debris cones (Sparkes et al., 2017, Finlayson, 2020, BGS, 2020). Past debris-flows have been linked to high-intensity rainfall (Winter et al., 2019b).

On average 4,000 vehicles cross the RabT per day (Winter et al. 2019a). Closures divert traffic ~88 km, if the Old Military Road (OMR), a one-way convoy diversion below the A83 is closed, casting a vulnerability shadow over 4,300 km^2 (Fig 1A). A full road closure costs ~£90k per day (2012 prices; Winter et al. 2019a) and £13.3m has been spent on protecting the A83 and improving the OMR (Scottish Parliament, 2020). Some debris-flows still exceed mitigation measures and impact the A83 and OMR. Quantified RabT risk studies justified measures for the LMP (Winter at al., 2008; Winter and Wong, 2020) which sends out daylight patrols and activates warning ‘wig-wag’ lights on the RabT approach if forecast rainfall is >=25 mm in a 24-hour period or >=4 mm in a 3-hour period (Winter et al. 2020).

LANDSLIDE ACTIVITY

A new RabT landslide inventory has been collated from road reports (2003-2015), quarterly and event responsive terrestrial laser scans (TLS; 2015-2019) and time-lapse imagery (2017-2020). Post-2015 it is unlikely events are missing as TLS (0.1 m resolution) and time-lapse imagery was used (Sparkes et al., 2017 and this study). Pre-2015, debris-flows that reached the A83 are recorded, but smaller landslides may not be. From 2003 to 2019 there were 63 landslides (Fig. 1); 43 were debris-flows (19 HDFs, 21 CDFs, three of unknown type), 11 slope creeps, and nine soil falls. 15 debris-flows closed the A83, on average nearly once a year since 2003; six reached the OMR.

60 landslides have known source areas (Fig. 1B), 45% (n=27) are in till, 35% (n=21) in debris cones and 20% (n=12) in regolith. 50 of these have source volumes derived from TLS (2015-2019) or estimates from reports (2007-2015). Debris cones cover 22% of the slope and account for 27% of the landslide volume; regolith (18% of the slope) and till (61% of the slope) account for 10% and 62% of the landslide volume respectively. Volumetric contributions from different materials reflect failure processes and depth to bedrock. Debris cone sources have deep scarps which shallow downslope, indicative of rotational slides. Till and regolith sources have a regular depth profile indicating translational failures. Modelling over a TLS derived DEM shows coupling of source areas and stream flow (Fig. 1B).

MANAGING DEBRIS-FLOW RISK - MONITORING STRATEGIES FOR ALERT, TRACKING AND DETECTION

Here we use 2018, an active year with 19 of the 63 landslides (Fig 1C), as a case study for pro-active, near-real-time monitoring to alerting stakeholders to increased landslide risk based on rainfall thresholds, tracking slope creep and detecting debris-flows occurrence.

Rainfall on seasonal, daily and 15-minute timescales are used to indicate raised landslide risk. The 2013-2019 seasonal rainfall trend was examined for Scottish Environment Protection Agency (SEPA) RabT rain gauge data (SEPA, 2020) using the Bayesian Estimator of Abrupt change, Seasonality and Trend (BEAST) analysis package (Zhao et al., 2019). BEAST uses ensemble modelling, where multiple competing models analyze data, and Bayesian statistics derive a model average with associated probabilities that detect if seasonal and trend changes are 'true'.

An Antecedent Precipitation Index (API; Fedora and Beschta, 1989), a proxy for ground saturation (Segoni et al., 2018), was calculated for daily rainfall totals using Equation 1, as an indicator of raised debris-flow risk.

$$API_i = k(API_{i-1}) + P_i \qquad (1)$$

Where API_i is the API at time i, P_i is the daily rainfall total at i and k is a constant decay function defined by the user (k=0.8). Rainfall was measured with an on-slope Davis Vantage Pro 2 gauge, better reflecting on-slope conditions than the off-slope SEPA gauge.

An intensity-duration (I-D) threshold was developed using 15-minute rainfall intensity data. Duration and mean rain intensity for all storms in the study period were plotted (Brunetti et al., 2010; Guzzetti et al., 2008), with a six-hour inter-event period. An I-D threshold above which landslides occur was visually derived from the results. Mean rain intensity over an entire storm was used as not all landslide timings were known.

Alerts of slope changes allow stakeholders to be on stand-by, pre-position resources, or proactively manage risk. Processing of time-lapse imagery in a particle image velocimetry tool (PIVLab; Thielicke and Stamhuis, 2014; Thielicke, 2020) detected creep on the 19/09/2018. Displacement vectors and velocity were established between consecutive slope-wide images at 16x16 pixel resolution (~2.7 m^2). Cumulative deformation was derived for a point tracked through the photo sequence. Inverse velocity (I-V), a tool used to predict failure in brittle materials (Carlà et al., 2017), was used as a tentative metric for till failure prediction despite the non-brittle materials involved. Imminent failure is predicted when I-V values reach zero (infinite velocity). Time between images was not uniform due to poor visibility, so velocity data from PIVLab were interpolated to 12h intervals, with a moving average smoothing of 24h. I-V was calculated for smoothed data using Equation 2 (Manconi and Giordan, 2016), where I_v is inverse velocity and V_w is velocity (V) over the defined time window (w).

$$\boldsymbol{I_v = \frac{1}{V_w}} \qquad (2)$$

Seismics were used to detect debris-flow onset. Seismics are widely used in torrent debris-flows systems (Walter et al., 2017), but here a Raspberry Shake 3D seismometer (Raspberry Shake, 2020; Manconi et al., 2018) was deployed for detection on a hillslope with uncertain flow routing. The seismogram trace shows characteristic debris-flow signals, generated through clast-clast and flow-substrate interactions, above the long-term average. Hodograms (plotting signal direction through time) were used to confirm the direction of debris-flow signals to the seismometer. Hodograms are seldom used in geosciences but have been used in rockfall monitoring (Borella et al., 2019).

RAINFALL THRESHOLDS

BEAST identified three rainfall seasonal change points (SCP) in winter periods from 2013 to 2016 (Fig. 2A). SCP3 (Fig. 2A) is Storms Desmond and Frank which caused debris-flows at the RabT. No SCPs are seen from 2016-2019. However, debris-flows are coincident with abrupt rainfall trend change points (TCPs) 2, 6 and 7, their subsequent falling trends and in long period high trends (TCP1; Fig. 2B). TCP7 starts the 2018 landslide period. For this period Fig. 2C shows when LMP forecast rainfall thresholds were exceeded and 'wig-wag' warning lights were operating, along with the same thresholds plotted using on-slope, live rain data. False alarms and missed landslides account for 6.9% of the study period for wig-wags and 12.2% for on-slope data (Fig. 2D). Wig-wags are human operated, reducing false alarms through expert judgement. However, on-slope data would raise alert levels two times where landslides occurred, that are not fully covered by the wig-wags (Fig. 2C i and ii).

Landslide producing storms were medium (>10h) to long duration (max. 72h; Fig. 2E); for two storms it is not known in which the landslide happened. Mean rain intensity for landslide initiation ranges from 2.95 mm/hr to 8.15 mm/hr. Landslides occur above the threshold described by Equation 3.

$$I = 4.75D^{-0.18} \qquad (3)$$

Where *I* is mean rain intensity and *D* is duration. As all confirmed landslide storms were >10h duration, the threshold may not apply to <10h storms. The I-D threshold gives a false alarm for 5.7% of the study period (Fig. 2G).

All landslides (n=18) occur over an API threshold of 37 mm, with three false alarms and long periods of alert with no landslides (Fig. 2F). A 62 mm API threshold covers 90% of landslides (n=16), reduces false alarms to 0.8% of the study period (Fig. 2G), but misses two mid-December events. A combination of I-D and API thresholds maximizes landslide detection and minimizes false alarms (Fig 2G). All landslide inducing storms exceed the I-D threshold with five false alarms (Fig. 2F i to v) which API thresholds can reduce to two (Fig. 2F iv, v).

TIME-LAPSE VECTOR TRACKING

Creep of Failure 2 (Fig. 2B) was monitored via time-lapse image vector tracking from initiation (19/09/2018) to arrest (27/09/2018) using PIVLab (Thielicke and Stamhuis, 2014; Thielicke, 2020). Vectors of change and a velocity heat map between consecutive images are shown in Figures 3A and 3B.

Creep initiation coincides with a rainstorm on the 18/09/2018 (Fig. 3C i). Half of the total cumulative deformation occurs in the first 2.5 days. Inverse velocity (I-V) rapidly decreases towards zero on the 19-20/09/18; extrapolation of the I-V trend predicts failure on the 21/09/2018. However, I-V values increase on the 21/09, indicating reduced velocity after rainfall ceases. The deformation rate slows until arrest and subsequent rainfall does not affect the deformation rate (Fig. 3C ii and iii). Operationally, alert levels would be raised in Phase i when imminent failure seemed likely but lowered after the 21/09.

PASSIVE SEISMICS DEBRIS-FLOW DETECTION

Seismics identified a HDF (Figs. 4A and 4B) on the 09/10/2018 and located the source area. The z-axis seismogram (Fig. 4C) shows a high-amplitude signal lasting ~15s, corresponding with the failure time derived from time-lapse imagery, which is likely the HDF in motion. Short duration, lower amplitude signals follow and are likely post-landslide sediment and boulder reworking. Hodograms show very little activity at first (Fig. 4C i), but signal strength increases as the HDF signal arrives (ii) before subsiding (iii). Stacked hodograms, overlain on a DEM, point to the HDF source area as the direction of the incoming signal (Fig. 4D).

RabT debris-flow seismic signals are brief due to short, steep flow paths, with boulder and sediment reworking post-event. Another deposit on Fig. 4B, which is a thin, fine-grained drape but has a large deposit footprint, was not detected by seismics; indicating that whilst high debris content flows can be detected, hyper-concentrated flows may need larger station arrays for detection.

DISCUSSION AND CONCLUSIONS

This paper presents on-site monitoring at the RabT, aimed at supplementing the existing LMP (Winter et al., 2008). Between 2003 and 2019 there are 63 landslides recorded, including 43 debris-flows. Two landslide processes lead to debris-flows, shallow translational failures (mean depth *c*.1 m), generally below hydrological convergence zones in regolith and till, and deep-seated (>2 m) rotational failures in debris-cones. Material type exerts control on landslide volumes. Total material losses from the slope are 6,829 m^3, with debris cones accounting for 27% (1,853 m^3), regolith 10% (697 m^3) and till the remaining 63% (4,278 m^3).

BEAST rainfall analysis shows that landslides are primarily associated with abrupt rainfall trend changes. In the 2018 study period, antecedent, and medium- to long-duration, high-intensity rainfall is shown to be an important factor in debris-flows initiation. New local API and I-D rainfall thresholds, identify all landslide inducing storms and minimize false alarms, improve on the LMP and provide road authorities time to consider actions. 90% of RabT landslides occurred over a 62mm API, indicating a critical antecedent rainfall threshold. Rainstorm I-D >10h is key for landslide initiation with largely higher mean rain intensity than non-landslide storms.

Shadow trials with confusion matrices against LMP thresholds are needed before full deployment.

Time-lapse vector tracking located and quantified creeping deformation in response to rainfall drivers. I-V calculations forecast imminent failure in the initiation phase, however creep slowed when rainfall ceased and arrested despite further rainfall. This method can detect slope movement and indicate times of heightened risk of failure for management authorities.

24-7 passive seismic detection and hodograms were used to identify a HDF. In this instance, and likely others due to short RabT flow paths, the 15 second event duration is too brief for live warnings but allows for 24/7 event detection and rapid response, outside of time-lapse image capture. Additional seismometers (now deployed) extend the range of detection and allow more traditional geo-location.

On-site sensor systems can indicate raised risk levels and landslide detection for authorities, improving their ability to act. Low-cost sensors can be replicated at high-risk sites and lower risk sites where cost-benefit would normally prevent monitoring. Increased high-intensity rainfall due to climate warming is expected in Scotland (UKCP, 2018) and more sites will have increased debris-flow risk; greater low-cost monitoring capacity is a necessary advancement.

ACKNOWLEDGMENTS

We thank NERC (NE/P000010/1, NE/T00567X/1), Research England (www.Pitch-in.ac.uk ‘SlopeRIoT’), Transport Scotland and the Scottish Road Research Board (SRRB) for funding. We also thank BEAR Scotland, GeoRope, Jacobs, Forestry and Land Scotland, Glencroe Farm and John Mather for research, access, and on-site support.

REFERENCES CITED

Badoux, A., Graf, C., Rhyner, J., Kuntner, R. and McArdell, B.W., 2009, A debris-flow alarm system for the Alpine Illgraben catchment: design and performance: Natural Hazards, 49, p.517-539, https://doi.org/10.1007/s11069-008-9303-x

BGS, 2020, Onshore GeoIndex, https://mapapps2.bgs.ac.uk/geoindex/home.html (accessed June 2020)

Borella, J., Quigley, M., Krauss, Z., Lincoln, K., Attanayake, J., Stamp, L., Lanman, H., Levine, S., Hampton, S., and Gravley, D., 2019, Geologic and geomorphic controls on rockfall hazard: how well do past rockfalls predict future distributions?: Natural Hazards and Earth System Sciences, 19, p.2249–2280, https://doi.org/10.5194/nhess-19-2249-2019.

Brunetti M.T., Peruccacci, S., Rossi, M., Luciani, S., Valigi, D. and Guzzetti, F., 2010, Rainfall thresholds for the possible occurrence of landslides in Italy: Natural Hazards and Earth Systems Science, 10, p.447-458, https://doi.org/10.5194/nhess-10-447-2010

Carlà, T., Intrieri, E., Di Traglia, F., Nolesini, T., Gigli, G and Casagli, N. 2017 Guidelines on the use of inverse velocity method as a tool for setting alarm thresholds and forecasting landslides and structure collapses: Landslides, 14, p.517-534, https://doi.org/10.1007/s10346-016-0731-5

Chen, J-C., Lin, C-W., and Wang, L-C., 2009, Geomorphic Characteristics of Hillslope and Channelized Debris Flows: A Case Study in the Shitou Area of Central Taiwan: Journal of Mountain Science, 6, p.266-273, https://doi.org/10.1007/s11629-009-0250-0

Fedora, M.A. and Beschta, R.L., 1989, Storm runoff simulation using an Antecedent Precipitation Index (API) model: Journal of Hydrology, 112, p.121-133, https://doi.org/10.1016/0022-1694(89)90184-4

Finlayson, A., 2020, Glacial conditioning and paraglacial sediment reworking in Glen Croe (the Rest and be Thankful), western Scotland: Proceedings of the Geologists' Association, https://doi.org/10.1016/j.pgeola.2020.02.007

Gertseema, M., Schwab, J.W., Blais-Stevens, A. and Sakals, M.E., 2009, Landslides impacting linear infrastructure in west central British Columbia: Natural Hazards, 48, p.59-72, https://doi.org/10.1007/s11069-008-9248-0

Guzzetti, F., Peruccacci, S., Rossi, M. and Stark, C.P., 2008, The rainfall intensity–duration control of shallow landslides and debris flows: an update: Landslides, 5, p.3-17, https://doi.org/10.1007/s10346-007-0112-1

Huebl, J. and Fiebiger, G., 2005, Debris-flow mitigation measures, in Jakob, M. and Hungr, O., eds., Debris-flow Hazards and Related Phenomena, p.445-487, Springer, Berlin Heidelberg

Hungr, O., Leroueil, S. and Picarelli, L., 2014, The Varnes classification of landslide types, an update: Landslides, 11, p.167-194, https://doi.org/10.1007/s10346-013-0436-y

Manconi, A., Coviello, V., Galletti, M. and Seifert, R., 2018, Short Communication: Monitoring rockfalls with the Raspberry Shake: Earth Surface Dynamics, 6, p.1219-1227, https://doi.org/10.5194/esurf-6-1219-2018

Manconi, A. and Giordan, D., 2016 Landslide failure forecast in near-real-time, Geomatics: Natural Hazards and Risk, 7:2, p.639-648, https://doi.org/10.1080/19475705.2014.942388

Meyer, N., Schwanghart, W., Korup, O. and Nadim, F., 2015, Roads at risk: traffic detours from debris flows in southern Norway: Natural Hazards and Earth System Science, 15, p.985-995, https://doi.org/10.5194/nhess-15-985-2015

McMillan, F.N. and Holt, C.A., 2018, BEAR Scotland NW trunk road maintenance: efficient management of geotechnical emergencies: Quarterly Journal of Engineering Geology and Hydrogeology, 52, p.286-294, https://doi.org/10.1144/qjegh2018-035

Milne, F.D., Werritty, A., Davies, M.C.R. and Brown, M.J., 2009, A recent debris flow event and implications for hazard Management: Quarterly Journal of Engineering Geology and Hydrogeology, 42, p.51–60, https://doi.org/10.1144/1470-9236/07-073

Raspberry Shake, 2020, https://raspberryshake.org/ (accessed June 2020)

Segoni, S., Rosi, A., Lagomarsino, D., Fanti, R. and Casagli, N., 2018, Brief communication: Using averaged soil moisture estimates to improve the performances of a regional-scale landslide early warning system: Natural Hazards and Earth System Science, 18, p.807-812, https://doi.org/10.5194/nhess-18-807-2018

SEPA, 2020, Rest and Be Thankful daily rainfall record. https://www2.sepa.org.uk/rainfall/ (accessed May 2020)

Sparkes, B., Dunning, S., Lim, M. and Winter, M.G., 2017, Characterisation of Recent Debris Flow Activity at the Rest and Be Thankful, Scotland, in Mikoš, M., Vilímek, V., Yin, Y. and Sassa, K., eds., Advancing Culture of Living with Landslides, Volume 5 Landslides in Different Environments: WLF: Workshop on World Landslide Forum Conference Proceedings, p.51-58, https://doi.org/10.1007/978-3-319-53483-1_8

Scottish Parliament, 2020, Official Report of the Public Petitions Committee, 05 March 2020, http://www.parliament.scot/parliamentarybusiness/report.aspx?r=12561 (accessed, July 2020)

Thielicke, W., 2020, PIVlab - particle image velocimetry (PIV) tool, https://www.mathworks.com/matlabcentral/fileexchange/27659-pivlab-particle-image-velocimetry-piv-tool, MATLAB Central File Exchange. (Accessed July 2020)

Thielicke, W. and Stamhuis, E.J., 2014, PIVlab – Towards User-friendly, Affordable and Accurate Digital Particle Image Velocimetry in MATLAB: Journal of Open Research Software, 2 (1), p.e30. http://doi.org/10.5334/jors.bl

UKCP, 2018, UK Climate Projections. Met Office, https://www.metoffice.gov.uk/research/approach/collaboration/ukcp/ (accessed June 2020)

Vagnon, F., 2020, Design of active debris flow mitigation measures: a comprehensive analysis of existing impact models: Landslides, 17, p.313-333, http://doi.org/10.1007/s10346-019-01278-5

Walter, F., Burtin, A., McArdell, B., Hovius, N., Weder, B., Turowski, J.M., 2017, Testing seismic amplitude source location for fast debris-flow detection at Illgraben, Switzerland: Natural Hazards and Earth System Science, 17, p.939-955, https://doi.org/10.5194/nhess-17-939-2017

Winter M.G., Macgregor F., Shackman, L., 2008, Scottish Road Network Landslides Study: Implementation, The Scottish Executive, Edinburgh

Winter, M.G., Peeling, D., Palmer, D. and Peeling, J., 2019a, Economic impacts of landslides and floods on a road network. AUC Geographica, 54 (2), p.207-220, https://doi.org/10.14712/23361980.2019.18

Winter, M.G., Ognissanto, F. and Martin, L.A., 2019b, Rainfall Thresholds for Landslides Deterministic and Probabilistic Approaches: Transport Research Laboratory Published Project Report PPR901, https://trl.co.uk/reports/rainfall-thresholds-landslides

Winter, M.G., Kinnear, N. and Helman, S., 2020, A technical and perceptual evaluation of a novel landslide early warning system: Proceedings, Institution of Civil Engineers (Transport), https://doi.org/10.1680/jtran.19.00138

Winter, M.G. and Wong, J.C.F., 2020. The assessment of quantitative risk to road users from debris flow: Geoenvironmental Disasters, 7(4), p.1-19. DOI: https://doi.org/10.1186/s40677-019-0140-x

Zhao, K., Wulder, M.A., Hu, T., Bright, R., Wu, Q., Qin, H., Li, Y., Toman, E., Mallick, B., Zhang, X. and Brown, M., 2019, Detecting change-point, trend, and seasonality in satellite time series data to track abrupt changes and nonlinear dynamics: A Bayesian ensemble algorithm: Remote Sensing of Environment, 232, https://doi.org/10.1016/j.rse.2019.04.034

Zimmerman, F., McArdell, B.W., Rickli, C. and Scheidl, C., 2020, 2D Runout Modelling of Hillslope Debris Flows, Based on Well-Documented Events in Switzerland: Geosciences, 10, 70, https://doi.org/10.3390/geosciences10020070

FIGURE CAPTIONS

Figure 1. RabT landslide inventory. (A) Site regional context. Vulnerability shadow outlined in orange (modified from Winter et al. 2019a). (B) TLS derived hillshade and 2007 to 2019 landslide source areas, coloured by autumn-winter season (Sept-Feb), Spring (Spr) or Summer (Sum). Dashed lines delineate

surface material (modified from Finlayson, 2020). Landslide numbers refer to Figure 2. (C) 2003 to 2019 cumulative landslide timeseries and yearly totals.

Figure 2. (A) BEAST seasonal rainfall trend. (B) BEAST rainfall trend. (C) 01/09/18 to 31/12/18 landslide timeline. (D) Wig-wag and on-slope alert operation confusion matrix. (E) September to December rainstorm intensity-duration (I-D) plot. (F) Antecedent Precipitation Index (API) with 37 mm and 62 mm thresholds. Rainfall intensity (data loss 13/11-05/12) with storms >10h duration exceeding the I-D threshold. (G) API and I-D threshold confusion matrix.

Figure 3. (A) PIVLab deformation vector plot (Thielicke and Stamhuis, 2014). (B) Velocity heat map. (C) Cumulative rainfall, cumulative deformation and I-V.

Figure 4. (A) Pre-failure HDF source and seismometer location. (B) Post-failure. (C) Fifteen-minute seismogram with HDF signal (red box) and three hodogram time-steps (i, ii, iii). (D) Hillshade with HDF location and ten second stacked hodogram.

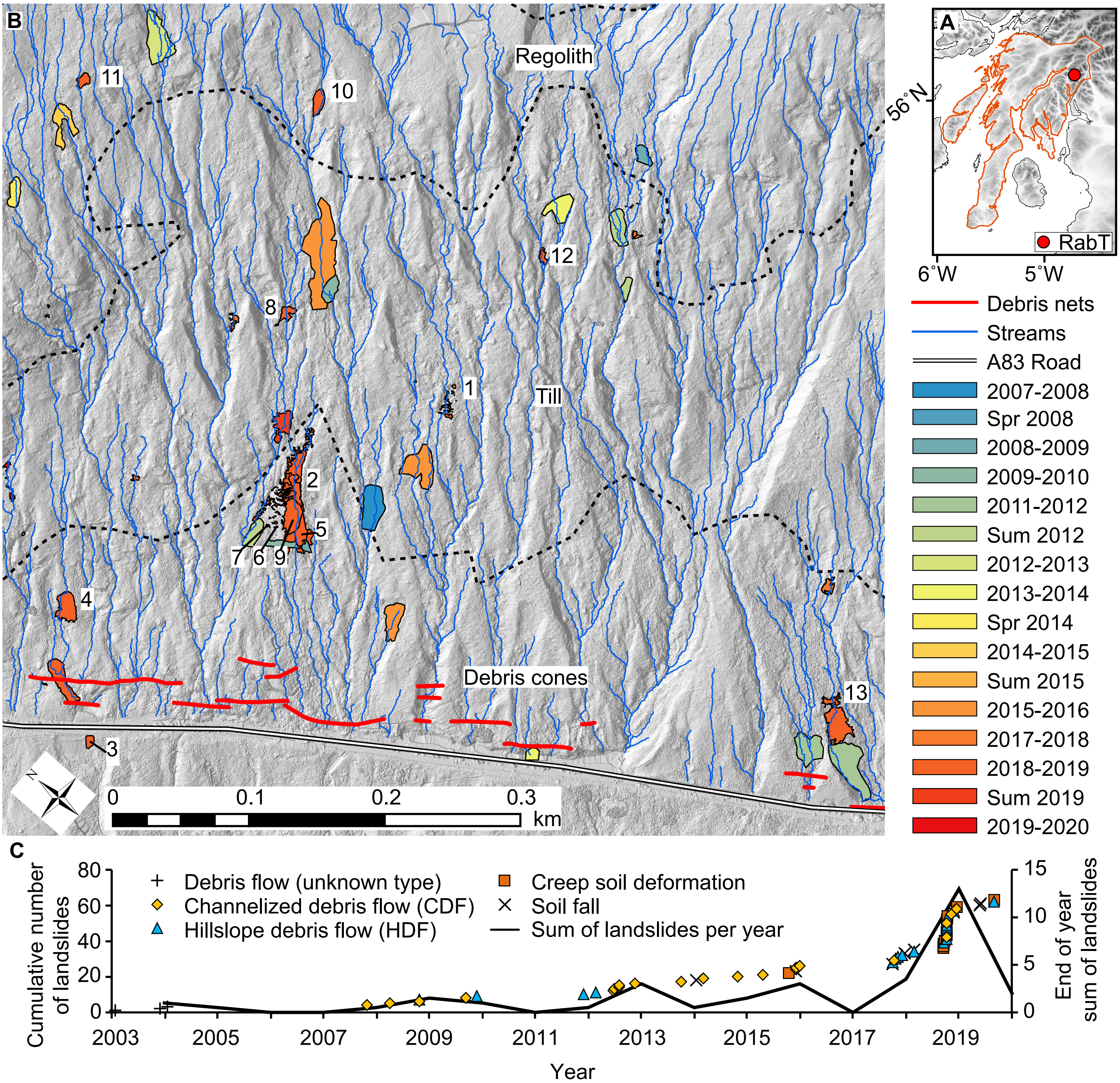

FIGURE 1
Author - Bainbridge et al.,

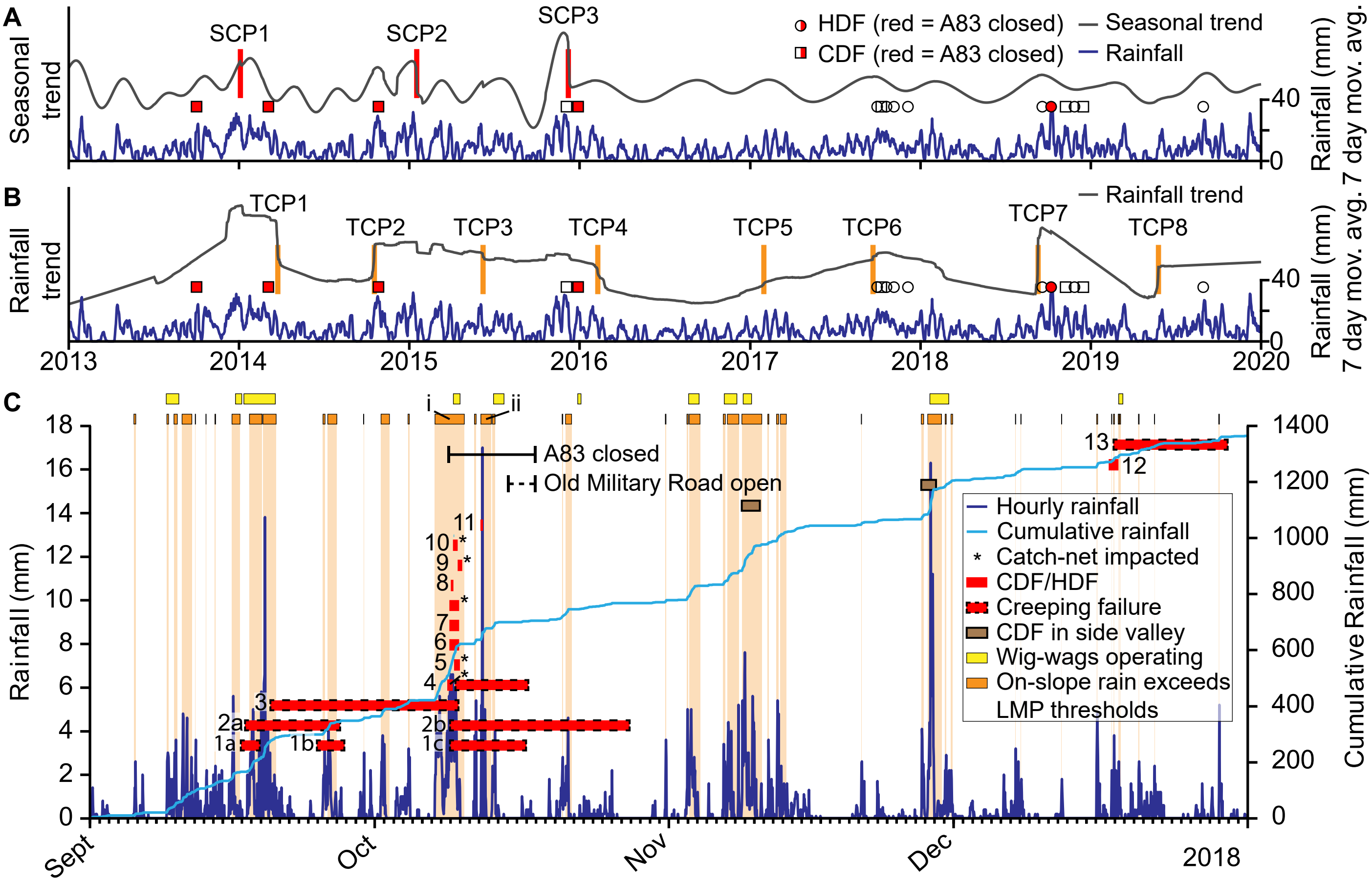

D

% of study period	Landslide		No landslide	
Wig-wags/On-slope on	**6.6%**	7.7%	**4.1%**	11.1%
Wig-wags/On-slope off	**2.8%**	1.1%	**86.5%**	80.1%

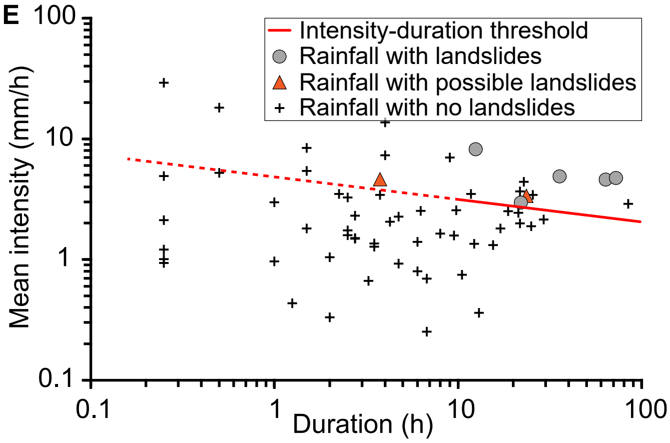

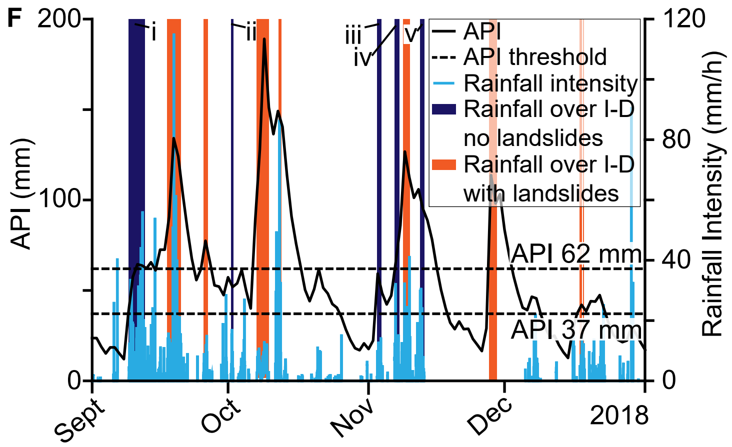

G

% of study period	Landslide		No landslide	
API/I-D > threshold	**29.5%**	8.2%	**0.8%**	5.7%
API/I-D < threshold	**3.3%**	0.0%	**81.0%**	86.1%

FIGURE 2

Author - Bainbridge et al.,

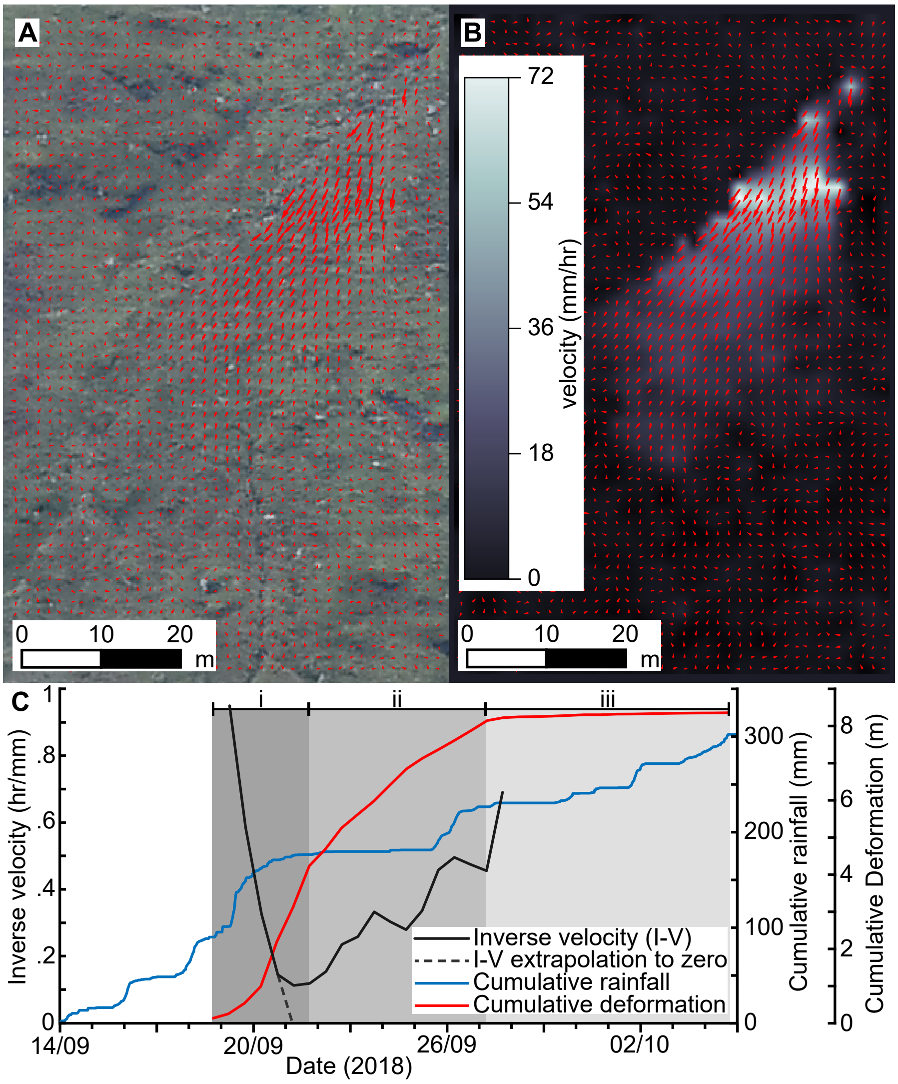

FIGURE 3
Author - Bainbridge et al.,

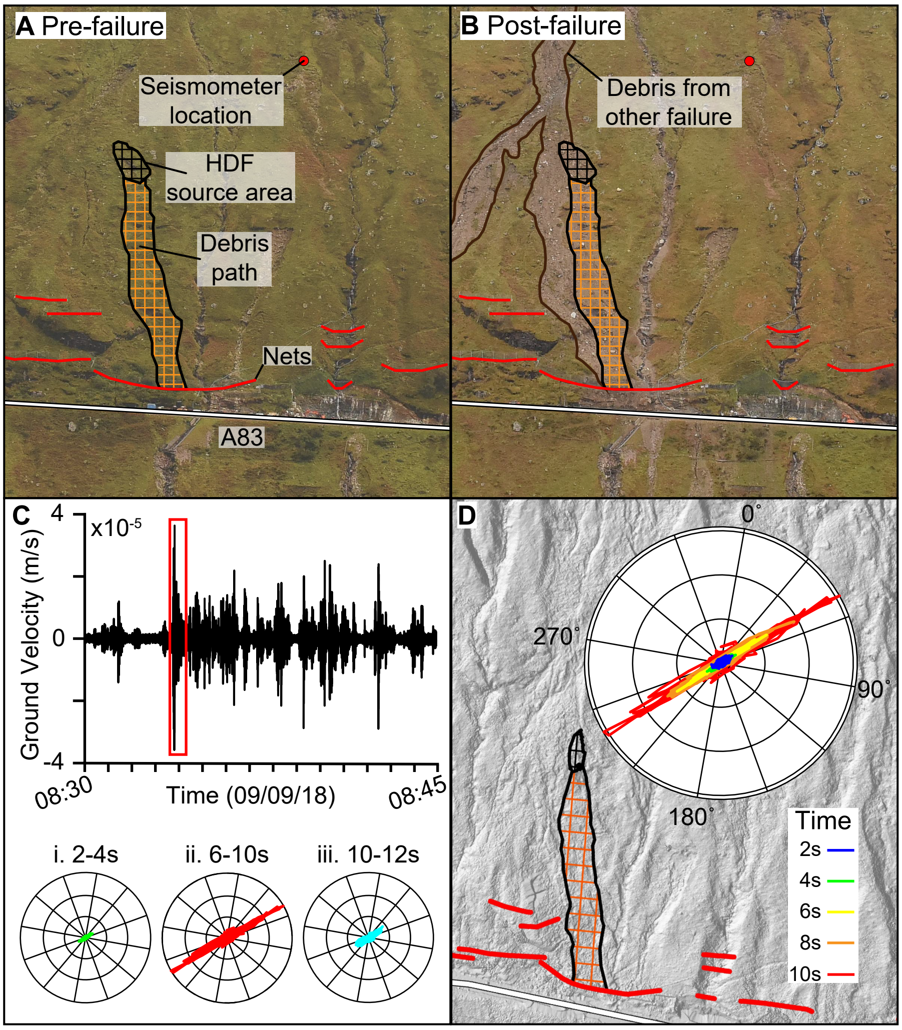

FIGURE 4
Author - Bainbridge et al.,